Microporous and Mesoporous Materials 127 (2010) 167–175

Contents lists available at ScienceDirect

Microporous and Mesoporous Materials

journal homepage: www.elsevier.com/locate/micromeso

Synthesis of hierarchical porous zeolite NaY particles with controllable particle sizes

Yi Huang [a], Kun Wang [b], Dehua Dong [a], Dan Li [a], Matthew R. Hill [c,d], Anita J. Hill [c], Huanting Wang [a,*]

[a] Department of Chemical Engineering, Monash University, Clayton, Victoria 3800, Australia
[b] Department of Materials Engineering, Monash University, Clayton, Victoria 3800, Australia
[c] Commonwealth Scientific and Industrial Research Organization (CSIRO), Materials Science and Engineering, Private Bag 33, Clayton South, Victoria 3169, Australia
[d] School of Chemistry, University of Melbourne, Victoria 3010, Australia

ARTICLE INFO

Article history:
Received 8 April 2009
Received in revised form 3 July 2009
Accepted 11 July 2009
Available online 8 August 2009

Keywords:
Hierarchical porous structure
Zeolite nanocrystals
Zeolite spheres
Hydrothermal synthesis

ABSTRACT

Hierarchical porous particles aggregated from primary zeolite NaY nanocrystals were hydrothermally synthesized via a three-stage temperature control strategy, without adding any organic additives. The as-synthesized samples were characterized using powder X-ray diffraction (XRD), scanning electron microscopy (SEM), transmission electron microscopy (TEM), energy dispersive X-ray spectroscopy (EDX), N_2 sorption, particle size analysis and Fourier Transform Infrared (FT-IR) spectroscopy. The results show that the zeolite aggregate particles with sizes of 190–600 nm are composed of highly crystalline zeolite NaY nanoparticles in the size range of 20–80 nm. The particle sizes of hierarchical porous aggregates can be readily tuned by varying the alkalinity of the zeolite precursor gel without notably changing the sizes of the primary zeolite nanocrystals. N_2 sorption results show that zeolite NaY aggregate particles have microporosity and mesoporosity (30.8–57.6%). The hierarchical zeolite particles exhibit very good mechanical stability, and remain intact after ultrasonication for several hours.

1. Introduction

Zeolites are a class of microporous crystalline solids, and they have been widely used as catalysts, adsorbents, and ion-exchangers because of their superior thermal/hydrothermal stability, strong acidity, good shape-selectivity, and high ion exchange capacity [1–4]. The existence of uniformly distributed cavities and channels in molecular dimensions, typically in the size range of 3–10 Å, endows zeolites with unique molecular recognition, discrimination, and organization properties [5]. However, in some cases, these intricate micropores in large crystals are less accessible, resulting in a significantly decreased mass transport rate of the guest species. This has been one of the main limitations for the utilization of zeolites. Therefore, considerable efforts have been devoted to alleviating the diffusion limitation due to the relatively small micropores of zeolites. The reduction of the particle size from microns to nanometers is recognized as an efficient way towards significantly shortened diffusion path lengths, substantially increased external surface area and more exposed active sites [6–9]. For instance, in petroleum cracking and reforming processes, the utilization of nano-sized zeolites reduces the mass and heat transfer resistance, and thus improves the catalytic selectivity and diminishes the coke formation [9–11]. Preparations of zeolite nanocrystals are often performed in a clear aluminosilicate solution or gel in the presence of organic templates/additives, and a number of zeolite nanocrystals have been successfully synthesized, such as zeolite A [7,12–14], sodalite [15,16], silicate-1 [8,17–19] and faujasite (X or Y) [14,18,20–22]. Recently, confined-space synthesis has been considered as an attractive approach for the synthesis of zeolite nanocrystals because of its size-tailorability [7,23–25]. Our recent work also demonstrated that zeolite nanocrystals with tunable particle sizes could be easily fabricated by employing a mesoporous carbon confined space method [26]. However, use of these nano-sized materials at the industrial scale seems to be a formidable challenge because of the difficulties in separation and recovery.

Hierarchical porous zeolites with combined micro/meso/macroporosities have attracted much attention since they combine the benefits of all pore-size regimes and have already been proven to be beneficial for both mass transport and separation [27,28]. The development in hierarchical porous zeolites has largely extended their practical applications, and become one of the most promising ways to circumvent the diffusion limitations in catalysis. For instance, in some catalytic reactions, the mass transport can be dramatically accelerated because of the easy accessibility of the additional pore systems (meso- or macro-pores). Generally, hierarchical porous zeolites can be prepared by adopting the following two main synthesis schemes: (1) synthesis of mesoporous zeolite single crystals by the postsynthesis treatments such as dealumination [29–31], desalination [32], steaming and alkaline leaching [31] or some newly developed direct-mesopore-incorporated methods

* Corresponding author. Tel.: +61 3 9905 3449; fax: +61 3 9905 5686.
E-mail address: huanting.wang@eng.moansh.edu.au (H. Wang).

1387-1811/$ - see front matter © 2009 Elsevier Inc. All rights reserved.
doi:10.1016/j.micromeso.2009.07.026

such as single-step hydrothermal synthesis with secondary-templating silylated polymers or amphiphilic organosilane [33,34], in situ sugar decomposition [35] and carbon confined-space synthesis [36–38]; (2) construction of zeolitic hierarchical structures from zeolite nanocrystals by using different methods, such as resin macro-templating [39], transitional templating using carbon [40] or mesoscale cationic polymers [10,41], gel casting of colloidal zeolite suspension [42], semi-zeolitic transformation of porous amorphous silica materials [43,44] and recrystallization of self-assembling zeolite seeds templated by polystyrene spheres [45]. Most of the hierarchical porous zeolitic materials reported in the above works are easily separated and recovered by, for example, filtration. However, they may more or less exhibit some drawbacks such as the complicated synthetic procedures, low mechanical strength after template removal, and use of expensive and unrecyclable organic templates. Therefore, it is of great interest to pursue alternative routes for the synthesis of hierarchical porous zeolitic materials without any organic additive and post-treatments.

More recently, mesoporous aggregates have been successfully fabricated without any secondary templates by carefully controlling the H_2O/SiO_2 supersaturation of the precursors [46]. This work has opened up a new possible way towards mass production of the hierarchical zeolites at low cost. Small zeolite NaY crystals were synthesized by Sang et al. using a two-stage temperature control method [47]. Valtchev and Bozhilov suggested that in a high alkaline system the aggregation mechanism would dominate during the period of NaY crystal growth at room temperature [5]. Based on this finding, they successfully prepared 100–300 nm spherical NaY aggregates built up of 10–20 nm nanocrystals after 3 weeks of hydrothermal treatment. In the present work, we attempt to modify the synthesis procedures to synthesize hierarchical porous NaY particles in shorter times. We report here a modified three-stage temperature control method, which allows for the synthesis of hierarchical porous particles in around 4 days without adding any organic additive, pore-forming agents or seeding crystals. The mesoporosity and the particle sizes of the zeolite NaY particles can be also tuned without notably changing the sizes of zeolite nanocrystals.

2. Experimental details

2.1. Zeolite synthesis

All chemicals were directly used as received without any further purification. The reactants used were sodium hydroxide pellets (99%, Sigma–Aldrich), 30 wt.% aqueous colloidal silica (Ludox HS-30, Sigma–Aldrich), aluminum isopropoxide (98 wt.%, Sigma–Aldrich) and doubly-deionized (DDI) water.

The molar composition of the gel used for the preparation of hierarchical porous NaY zeolites was $9.6Na_2O{:}1.0Al_2O_3{:}14.4SiO_2{:}\alpha\varpi H_2O$ (α = 175.3, 198.0, 220.7, 243.4, 288.8 and 334.2); the water to silica molar ratio ($n_{H_2O/Si}$) was calculated to be 12.2, 13.8, 15.3, 16.9, 20.1 and 23.2, respectively. The synthesized zeolite NaY was then denoted Y-nH_2O. Typically, in the synthesis of Y-$20.1H_2O$, 9.49 g of sodium hydroxide was added into a clean polypropylene (PP) bottle containing 37.50 g of DDI water. After the complete dissolution of sodium hydroxide, 5.00 g of aluminum isopropoxide was added under agitation for 2 h to yield sodium aluminate solution. In the meantime, 35.25 g of aqueous colloidal SiO_2 solution was weighed and slowly poured into the freshly prepared sodium aluminate solution under vigorous stirring. The mixture immediately turned into a milky gel, which possessed very low viscosity. The PP bottle was then tightly sealed. The initial gel system was subject to a three-stage crystallization to form NaY aggregate particles. At the first stage (initial aging), the PP bottle was transferred to a 25 ± 1 °C oil bath and aged for 24 h with constant stirring at 650 rpm. Secondly, the one-day aged precursor was then moved into a preheated oven set at 38 °C and further aged for another 24 h. At the final-stage, the precursor gel was hydrothermally treated at 60 °C for 48 h. For convenience, the term *three-stage synthesis* is used in this paper.

All the products were readily recovered by low-speed centrifugation, followed by washing with DDI water until pH = 8–9, and drying at room temperature for 48 h.

For comparison, commercial NaY zeolite (CBV-100) was purchased from Zeolyst International and used as the reference.

2.2. Characterization

X-ray powder diffraction (XRD) patterns were recorded on a Philips PW1140/90 diffractometer using Cu Kα target (40 kV, 25 mA) at a scan rate of $1^\circ\ min^{-1}$ with a step size of 0.02°, and at 2θ angles ranging from 4° to 40°. Scherrer's equation was employed to estimate the primary size of NaY crystals. The full-width at half maximum (fwhm) was determined at the peaks of 6.19° (1 1 1), 15.61° (3 3 1), and 23.58° (5 3 3) [9] using NaY zeolite (CBV-100) as the reference.

Scanning electron microscope (SEM) micrographs were taken with a JEOL JSM-6300F scanning electron microscope (15 kV). The energy dispersive X-ray spectrometer (EDXS) attached to the SEM was used to conduct elemental analysis of the samples. The final SiO_2/Al_2O_3 ratios for each sample were obtained by taking the average of at least 10 measurements at different spots.

IR spectra were recorded on a Perkin–Elmer Spectrum 100 FT-IR spectrometer with samples pressed in KBr pellets. Nitrogen adsorption–desorption experiments were carried out at 77 K on a Micrometrics ASAP 2020 sorption analyzer. All samples were degassed at 250 °C prior to each measurement. The surface area was determined using Brunauer–Emmett–Teller (BET) method. The micropore volume, V_{micro}, and micropore size distribution were determined by the *t*-plot and density functional theory (DFT) method, respectively. The mesopore size distribution was calculated from the desorption branch using the Barrett–Joyner–Halenda (BJH) method. The total pore volume, V_{total}, was estimated from the desorption branch of the isotherm at $P/P_0 = 0.99$, assuming complete pore saturation. The microporosity of the synthesized sample was calculated using $V_{micro}\% = (V_{micro}/V_{total}) \times 100\%$ [20,46]. The percentage of mesopore volume was estimated using $V_{extra}\% = 1 - V_{micro}\%$. The external surface area was used to estimate the average nanoparticle size assuming that the crystals are cubic in shape [22]

$$D = 4061/S_{\text{external}}$$

where D is the diameter of the nanoparticle in nm and S_{external} is the external surface area in m^2/g.

The particle size analysis of NaY aggregated zeolite particles was performed by light scattering method with a Malvern Instruments (Malvern, UK) Zetasizer (Nano ZS series, ZEN 3600). All samples were dispersed in DDI water at a pH value of around 9, and were subject to ultrasonication for 10 min before analysis. Transmission electron microscopy (TEM) images were taken with a Philips CM20 with acceleration voltage of 200 keV.

3. Results and discussion

3.1. Effect of crystallization time

Our three-stage temperature control process is composed of (1) initial aging (25 °C, 1 day), (2) secondary aging (38 °C, 1 day) and (3) crystallization (60 °C, 2 days or more). To study the crystalliza-

tion process, small aliquots of the samples were taken out of the zeolite gel (Y-20.1H_2O) after 24 h (25 °C, initial aging), 53 h (38 °C, secondary aging), 75 h, 96 h, and 120 h (60 °C, crystallization), respectively. Prior to each sampling, the gel was thoroughly stirred to ensure its uniformity. The formation of hierarchical porous zeolitic structures was monitored by XRD, IR, SEM and N_2 sorption. The XRD did not detect any crystalline structure after secondary aging (53 h) (Fig. 1a). Some small but broad peaks, corresponding to FAU-type structure, such as (1 1 1), (3 3 1) and (5 3 3), were distinguishable after 75 h (Fig. 1b); however, the sample still contained a large amount of amorphous material. A very fast crystallization rate was observed between 75 h and 96 h treatment. A well-crystallized FAU sample was obtained after 96 h (Fig. 1c). Further prolonging the crystallization time to 120 h resulted in the intensified and narrowed diffraction peaks, suggesting the increase in the crystallinity and crystal size (Fig. 1d). Therefore, in our synthesis, well-crystallized FAU-type zeolites with small crystal sizes can be prepared in a reasonably short time (around 96 h) via our three-stage temperature control method.

The FT-IR spectra of samples are shown in Fig. 2. The samples after initial aging (25 °C, 24 h) and second-stage aging (38 °C, 53 h) exhibit similar spectra without characteristic FAU adsorption bands, indicating they are still amorphous sodium aluminosilicates [48,49]. IR spectra of the sample treated at 60 °C for 1 day (75 h) clearly show three FAU characteristic bands, which are double-ring vibration at 566 cm^{-1} and symmetric stretching bands at 687 cm^{-1} and 762 cm^{-1}. The absorption bands at around 1440 cm^{-1} and 1332 cm^{-1} weaken with time, indicating the amount of amorphous material in the sample gradually decreases. This is due to the progressive phase transformation of amorphous phase into crystalline FAU phase. The aged gel quickly crystallizes at this stage (crystallization stage), and all characteristic bands are gradually intensified with the increasing synthesis time. The bands for amorphous phase completely disappear and only pure FAU absorption bands are observed in the 120 h sample. The FT-IR results are in good agreement with the XRD results. Fig. 3a displays the SEM micrograph of the amorphous aluminosilicate gel (53 h). Some gel particles with irregular shapes are observed whereas other gel particles possess spherical shape with a wide size range from a few tens of nanometers to submicron. Valtchev and Bozhilov [5] studied a similar gel system and they proved the existence of nuclei wrapped by

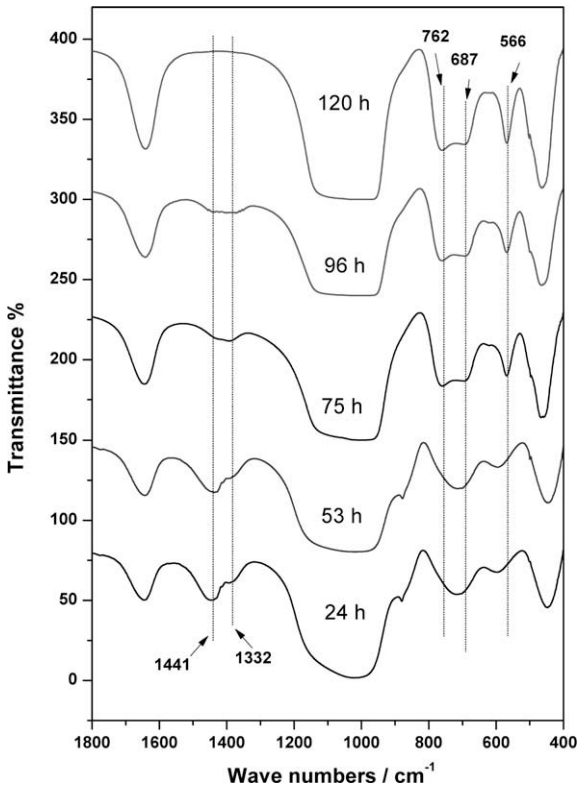

Fig. 2. IR spectra of samples taken out at (a) 24 h, (b) 53 h, (c) 75 h, (d) 96 h and (e) 120 h during the synthesis of Y-20.1H_2O.

amorphous mass, which could be verified by synchrotron in situ XRD. At 75 h, there are a large number of relatively uniform spherical particles in the size range of 100–250 nm (Fig. 3b). It is worth noting that these submicron-sized particles are composed of very small particles with sizes below 20 nm (Fig. 3b). However, these particles are poorly crystallized according to the XRD and IR studies. The SEM images of the 96 h sample are shown in Fig. 3c and d at different magnifications. At a low-magnification (Fig. 3c), very uniform spherical particles with sizes in the range of 200–

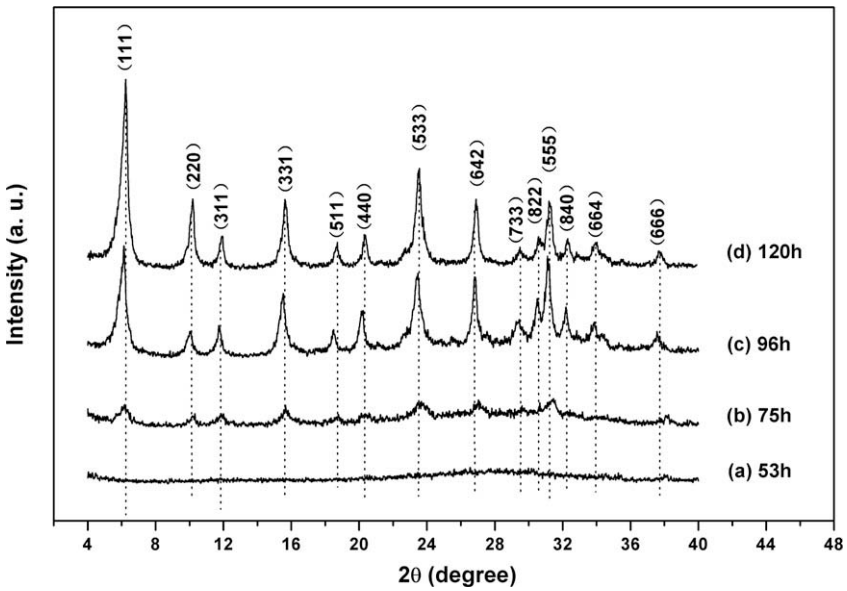

Fig. 1. XRD patterns of samples taken out at (a) 53 h, (b) 75 h, (c) 96 h and (d) 120 h during the synthesis of Y-20.1H_2O.

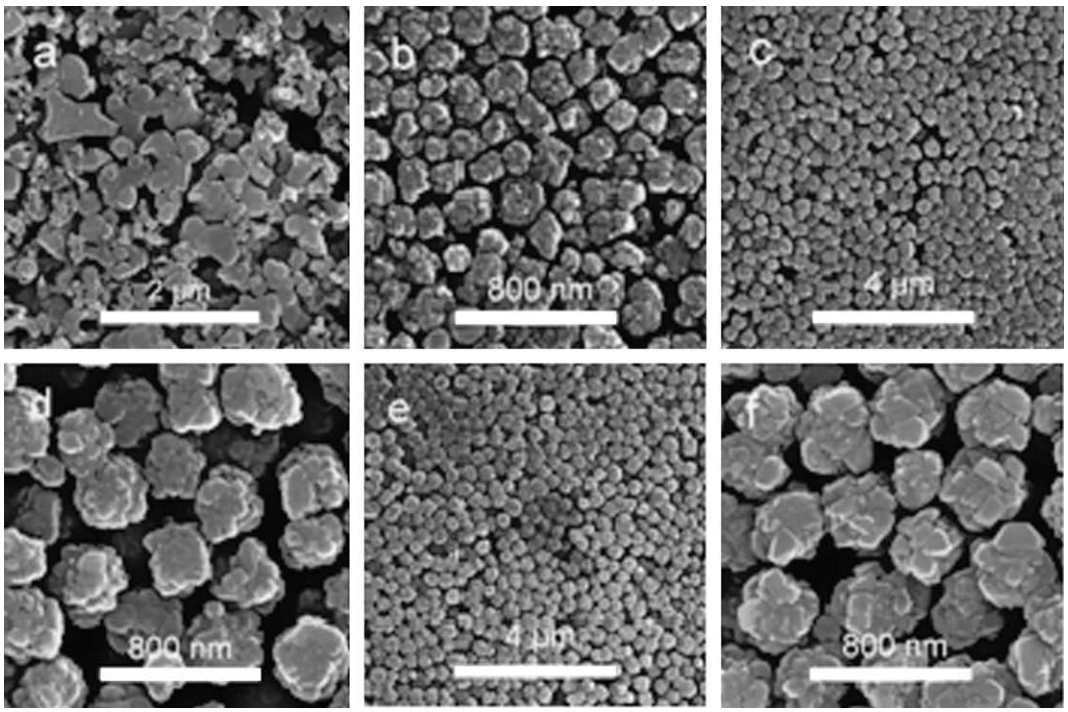

Fig. 3. SEM micrographs of samples from Y-20.1H_2O gel after (a) 53 h, (b) 75 h, (c and d) 96 h and (e and f) 120 h.

400 nm are observed. A close look at the sample reveals that the particles consist of closely aggregated nano-sized particles with sizes between 10 and 50 nm (Fig. 3d). This observation agrees well with the XRD results, in which very broad characteristic FAU diffraction patterns were obtained. Highly-crystallized porous particles (120 h sample) exhibit slightly larger particle sizes (300–600 nm, Fig. 3e) and nanocrystal sizes (20–80 nm, Fig. 3f) than the 96 h sample.

The 96 h and 120 h samples were analyzed by the nitrogen sorption technique, and the results are shown in Table 1 and Fig. 4. The 120 h sample shows higher BET surface area, micropore volume and total pore volume than the 96 h sample. This is because the 120 h sample has higher crystallinity, and slightly larger primary crystal sizes than the 96 h sample. In nitrogen sorption isotherms (Fig. 4a), both samples show a steep nitrogen uptake at very low relative pressures ($P/P_0 = 0.02$) corresponding to the filling of micropores. Higher N_2 adsorption capacity at low pressures is observed for 120 h sample, which is attributed to higher crystallinity. An obvious type H_4 hysteresis loop (from 0.40 to 0.85) is observed for both samples, signifying the filling of uniform slit-shaped intercrystal mesopores, which arise from the packing of zeolite nanocrystals. Another uptake appears at high relative pressure (0.85–1.0) for both samples, which is attributed to the filling of macropores formed by the packing of aggregated particles. Pore size distributions of the 96 h and 120 h samples are shown in Fig. 4b. Both samples show the hierarchical porous structures, which consist of mesopores (averaged at 3.5 and 10.7 nm) and intrinsic micropores (about 7.2 Å) arising from zeolite NaY. It is worth mentioning that that 96 h sample exhibits a higher mesoporosity than that of the 120 h sample in the pore size range of 2–24 nm. The formation mechanisms of relatively uniform sizes of the zeolite aggregate particles were well described in Ref. [5]. Briefly, the employment of low-temperature aging has been shown to have a very important influence on the formation of numerous nuclei [5,50]. In our method, a two-stage low-temperature (i.e., room temperature and 38 °C) aging was specially designed to favor the formation of a large number of nuclei, which then grew into nanoparticles at 60 °C by consuming surrounding amorphous gels via attachment of semi-crystalline units or amorphous gel particles to the crystalline centers; Such spontaneous mass crystallization in a very reactive gel system creates the chemical potential gradient, providing uniform driving force for nanoparticle aggregation. In addition, the sizes of the aggregated particles are greater than those (100–300 nm) obtained at room temperature for 3 weeks [5]. In our study, higher synthesis temperatures induced fast crystallization kinetics. The porous zeolite NaY particles were then produced by aggregation of nanocrystals with well-developed crystal faces.

Recently, Fang et al. [46] have reported that mesoporous ZSM-12 can be fabricated by simply evaporating a certain amount of water and alcohol from the synthesis solution before high-temperature crystallization. The final product was produced by orientated aggregation of zeolite nanocrystals, and it possessed a relatively high mesoporosity (~59% of total pore volume). The incorporation of a high-temperature evaporation process, however, is unsuitable for those zeolites requiring low-temperature crystallization. For example, SDA-free zeolite A is usually prepared at temperatures below 100 °C. Zeolite A quickly crystallizes into large single crystals during solvent evaporation. In our synthesis of hierarchical porous aggregated particles, vigorous agitation is employed to homogenize freshly mixed precursors at room temperature for 24 h. After this initial aging, the synthesis gel is heated to 38 °C, and further aged at this temperature for another 24 h (secondary aging), followed by a final-stage heat treatment (crystallization stage) at 60 °C for 48 h or more.

Table 1
N_2 adsorption–desorption results of the samples prepared from Y-20.1H_2O gel.

Samples (h)	S_{BET} (m^2/g)	$V_{micropore}$ (cm^3/g)	V_{total} (cm^3/g)	V_{micro} (%)
Y-96	598	0.21	0.34	61.5
Y-120	691	0.29	0.42	69.0

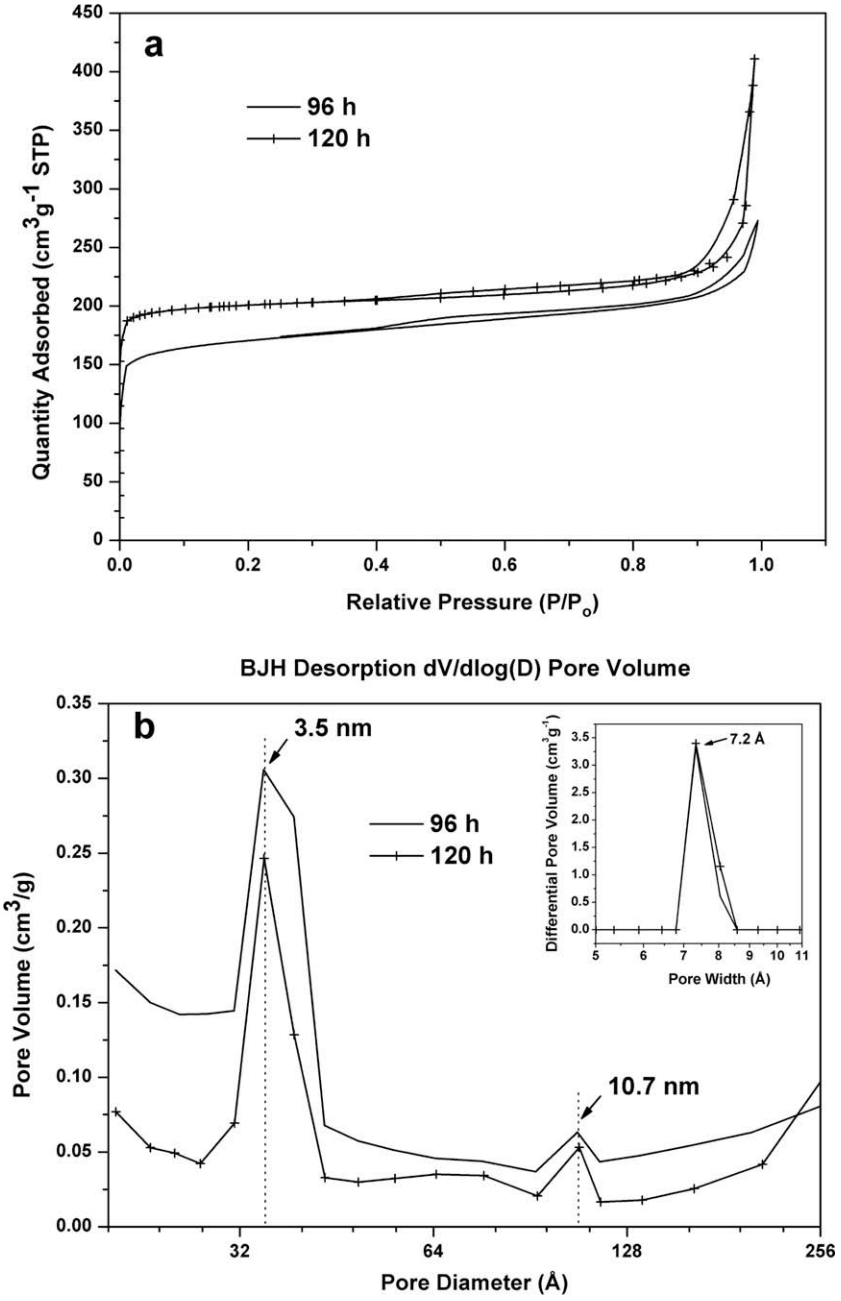

Fig. 4. N_2 adsorption–desorption isotherms (a) and BJH pore size distribution (b) of the samples prepared from Y-20.1H_2O gel. The inset is the micropore size distributions determined by the DFT method.

3.2. Effect of water content

Fig. 5 shows the XRD patterns of samples produced using different H_2O/SiO_2 molar ratios (12.2, 13.8, 15.3, 16.9, 20.1 and 23.2) under the same synthetic conditions. The XRD patterns indicate that all samples exhibit a FAU-type zeolite structure. Notably, the samples, typically Y-13.8H_2O, Y-15.3H_2O, Y-16.9H_2O and Y-20.1H_2O, show significantly broadened diffraction peaks, suggesting small sizes of the primary zeolite nanocrystals (Fig. 5b–e). The primary crystal size of each NaY sample was estimated by Scherrer's equation and summarized in Table 2. The primary crystal size is 33, 20, 15, 13, 18 and 45 nm for Y-23.2H_2O, Y-20.1H_2O, Y-16.9H_2O, Y-15.3H_2O, Y-13.8H_2O and Y-12.2H_2O, respectively. The primary nanocrystals with smaller sizes can be synthesized as the H_2O/SiO_2 molar ratio is in the range of 20.1–13.8. When the H_2O/SiO_2 molar ratio is increased to 23.2 or decreased to 12.2, the primary crystal size increases significantly. The primary crystal sizes listed in Table 2 were estimated using external surface areas measured by nitrogen sorption analysis. The calculated primary nanocrystal sizes of Y-$n$$H_2O$ samples lie between 30 and 60 nm, which are greater than those from XRD, but in good agreement with the data from TEM observations as described below.

The SEM micrographs of samples are displayed in Fig. 6. Y-$n$$H_2O$ samples (n = 13.8, 15.3, 16.9, 20.1 and 23.2) are fairly uniform in crystal size, and the individual aggregates are composed of closely packed nanocrystals, whose sizes vary from 10 to 80 nm and increase with increasing the value of n. This important observation confirms that the zeolite gel with lower water content favors the formation of smaller FAU zeolite nanocrystals. It is noted that the NaY zeolite particles prepared with higher silica concentration

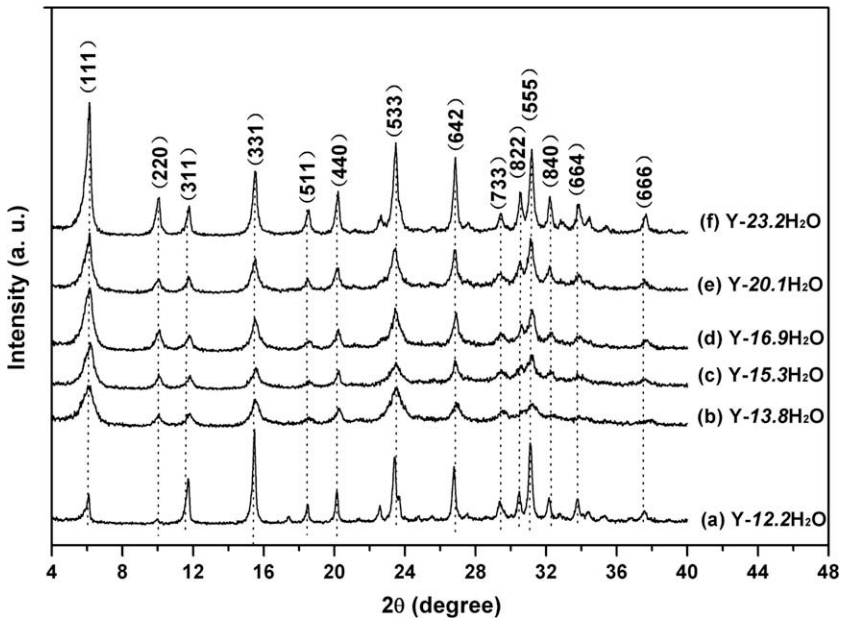

Fig. 5. XRD patterns of samples prepared from (a) Y-12.2H_2O, (b) Y-13.8H_2O, (c) Y-15.3H_2O and (d) Y-16.9H_2O, (e) Y-20.1H_2O and (f) Y-23.2H_2O prepared under the same synthetic conditions (24 h at 25 °C, 24 h at 38 °C and 48 h at 60 °C).

Table 2
Primary nanocrystal sizes and particle sizes of hierarchical porous aggregated NaY zeolite particles.

Samples	Crystallite size from XRD (nm)	Particle size from DLS (nm)	Primary nanocrystal size from BET area (nm)	Particle size from SEM (S) or TEM (T) (nm)
Y-23.2H_2O	33	620	50	600 ± 40 (S)
Y-20.1H_2O	20	358	34	400 ± 30 (S)/(T)
Y-16.9H_2O	15	247	40	280 ± 25 (S)/(T)
Y-15.3H_2O	13	236	38	250 ± 30 (S)/(T)
Y-13.8H_2O	18	220, 700	56	190 ± 30 (S)
Y-12.2H_2O	45	-	110	300 ± 40, 650 ± 50 (S)

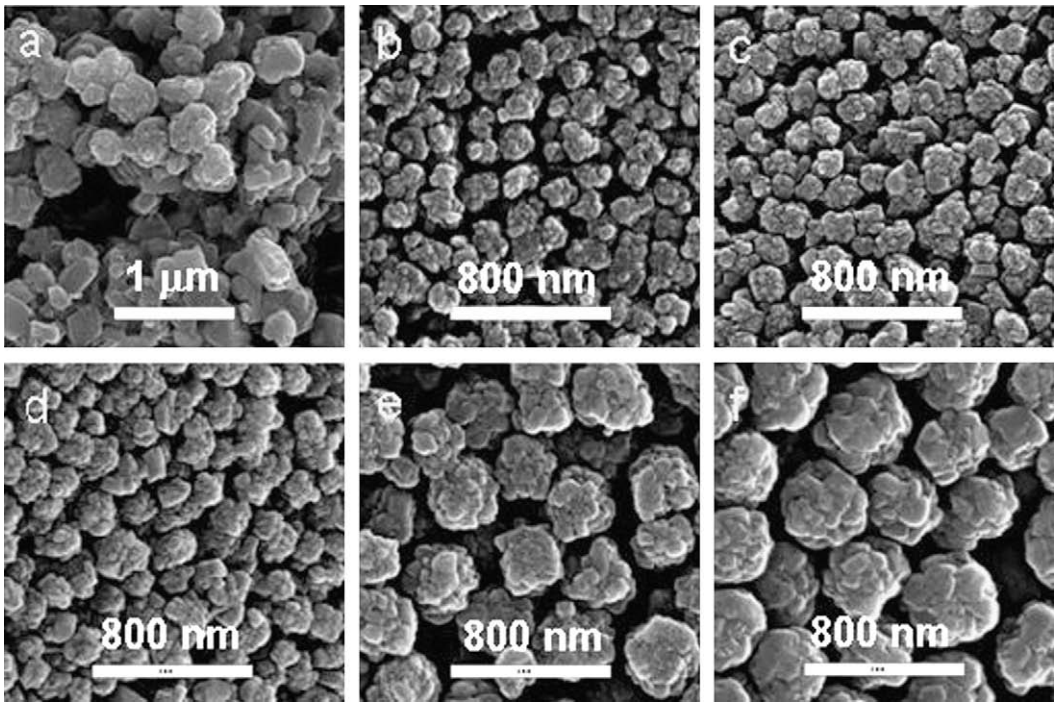

Fig. 6. SEM micrographs of samples of (a) Y-12.2H_2O, (b) Y-13.8H_2O, (c) Y-15.3H_2O and (d) Y-16.9H_2O, (e) Y-20.1H_2O and (f) Y-23.2H_2O prepared under the same synthetic conditions (24 h at 25 °C, 24 h at 38 °C and 48 h at 60 °C).

(i.e., small $n_{H_2O/Si}$) have smaller average aggregate sizes except for Y-12.2H_2O, in which submicron-sized single crystals and porous aggregates coexist (Fig. 6b). This is probably because less uniform crystallization occurred in Y-12.2H_2O gel. For each Y-$n$$H_2O$ sample, the average particle (aggregate) size was estimated from at least 500 particles in the SEM or TEM images, and listed in Table 2. The aggregate size gradually decreases from 600 ± 40 (Y-23.2H_2O) to 190 ± 30 nm (Y-13.8H_2O), and then suddenly increases to 300 ± 40/650 ± 50 nm for Y-12.2H_2O.

The particle size distributions of hierarchical porous FAU zeolite particles were further analyzed by the light scattering method. Y-$n$$H_2O$ samples with n between 13.8 and 23.2 were demonstrated, and their particle size distributions are shown in Fig. 7. Y-23.2H_2O, Y-20.1H_2O, Y-16.9H_2O and Y-15.3H_2O exhibit unimodal size distributions whereas Y-13.8H_2O possesses a bimodal size distribution (Fig. 7). The reason for the formation of large congregated agglomerates in Y-13.8H_2O might be due to the relatively high alkalinity of the gel which induces non-uniform aggregation of zeolite nanocrystals. The particle sizes of the aggregate particles remain unchanged even after sonication for several hours, demonstrating they are mechanically strong. The sizes of Y-$n$$H_2O$ zeolites are listed in Table 2 and of the peak particle size is 220, 236, 247, 358 and 620 nm for Y-13.8H_2O, Y-15.3H_2O, Y-16.9H_2O, Y-20.1H_2O and Y-23.2H_2O, respectively, matching well with those measured from SEM or TEM images. There is a good agreement between XRD, SEM and particle size distribution analysis data, which show that the average particle size decreased with decreasing water content ($n_{H_2O/Si}$).

The hierarchical porous FAU zeolite particles were also analyzed by the N_2 adsorption–desorption technique and the textual data are presented in Table 3. The BET surface areas of Y-$n$$H_2O$ zeolite samples decreases from 757 to 404 m^2/g when the water to silica molar ratio (n) decreases to 13.8; the BET surface area increases to 629 m^2/g when the n value becomes 12.2. The corresponding micropore volume shows a similar trend, i.e., it decreases from 0.3 m^3/g for Y-23.2H_2O to 0.14 m^3/g for Y-13.8H_2O and then increases to 0.27 m^3/g for Y-12.2H_2O. This may be explained by the fact that the hierarchical porous zeolite particles synthesized with n = 20.1–13.8 possess lower crystallinity as indicated by XRD and IR studies. The BET surface areas of Y-$n$$H_2O$ samples are fairly comparable to the NaY nanocrystals (23–50 nm) reported elsewhere [22]. In addition, the hierarchical porous FAU zeolite particles have relatively high total pore volumes ($\geqslant$0.33 m^3/g). The percentages of the mesopore volume (V_{extra}%) in each Y-$n$$H_2O$ sample are summarized in Table 3. Initially V_{extra}% increases with decreasing n value, especially in the cases of Y-15.3H_2O and Y-13.8H_2O whose mesopore volumes account for more than 50% of the total pore volume; V_{extra}% then largely decreases to 30.8% for Y-12.2H_2O. It is noted that micro-sized crystals usually exhibit an external surface area less than 5 m^2/g [9] and nano-sized crystals with about 45 nm in size have BET surface area of around 95 m^2/g [22]. In our case, the external areas are calculated to be 82, 120, 101, 106 and

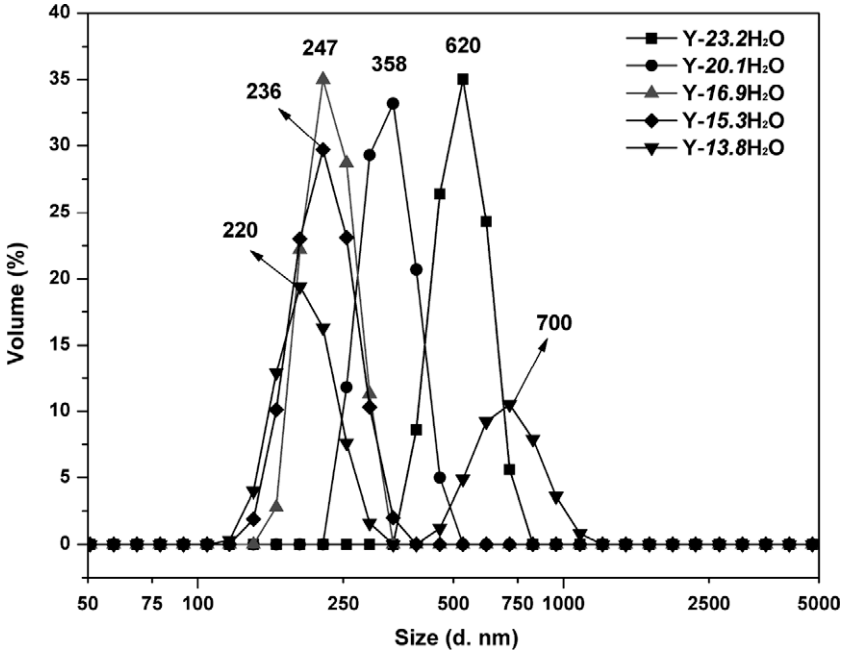

Fig. 7. Particle size distributions of Y-13.8H_2O, Y-15.3H_2O, Y-16.9H_2O, Y-20.1H_2O, and Y-23.2H_2O prepared under the same synthetic conditions (24 h at 25 °C, 24 h at 38 °C and 48 h at 60 °C).

Table 3
N_2 adsorption–desorption results and SiO_2/Al_2O_3 ratios of as-synthesized hierarchical porous NaY zeolite particles.

Samples	S_{BET} (m^2/g)	$S_{external}$ (m^2/g)	$V_{micropore}$ (cm^3/g)	V_{total} (cm^3/g)	V_{extra} (%)	SiO_2/Al_2O_3
Y-23.2H_2O	757	82	0.30	0.46	34.8	3.0
Y-20.1H_2O	598	120	0.21	0.34	38.3	3.3
Y-16.9H_2O	587	101	0.24	0.47	48.9	3.2
Y-15.3H_2O	506	106	0.18	0.39	53.9	3.2
Y-13.8H_2O	404	72	0.14	0.33	57.6	3.1
Y-12.2H_2O	629	37	0.27	0.39	30.8	3.6

72 m^2/g for Y-23.2H_2O, Y-20.1H_2O, Y-16.9H_2O, Y-15.3H_2O and Y-13.8H_2O, respectively, which are consistent with the expected values.

Furthermore, transmission electron microscopy (TEM) was used to observe the hierarchical structures of the synthesized zeolite particles. The representative TEM images of Y-13.8H_2O, Y-16.9H_2O and Y-20.1H_2O are shown in Fig. 8. The particle sizes obtained from the low-magnification TEM images are similar to those obtained from SEM and light scattering analysis (Fig. 8a, c and e and Table 3). The TEM images taken at high magnifications reveal the polycrystalline nature of these hierarchical porous particles, as they are composed of many closely packed nanocrystals with the average size of around 40 nm. It is noteworthy that most of the nanoparticles show different orientations, while some of the adjacent nanoparticles have the same orientation, which suggests a certain degree of intergrowth (Fig. 8b, d and f). The crystalline nature of these nanoparticles is confirmed by the existing lattice fringes with the *d* spacing of 0.72 nm, which is well known for FAU-type zeolite structure. Moreover, the elemental analysis experiments reveal the SiO_2/Al_2O_3 ratio of all hierarchical zeolite samples are higher than 3, which are in the range of Y-type zeolites (Table 3). Additionally, these hierarchical porous particles may be useful as catalysts and adsorbents, and templates or building units for the fabrication of other materials with multi-modal porosity.

4. Conclusions

We have demonstrated that hierarchically porous aggregated particles consisting of well-crystallized primary zeolite NaY nanocrystals can be synthesized using our three-stage temperature control method without adding any organic additive, pore generating agents or seeding crystals. The particle sizes and multi-modal porosity of zeolite NaY particles can be controlled by carefully varying the water to silica molar ratio of the synthesis gel. Importantly, the synthesis method reported in this paper is cost-effec-

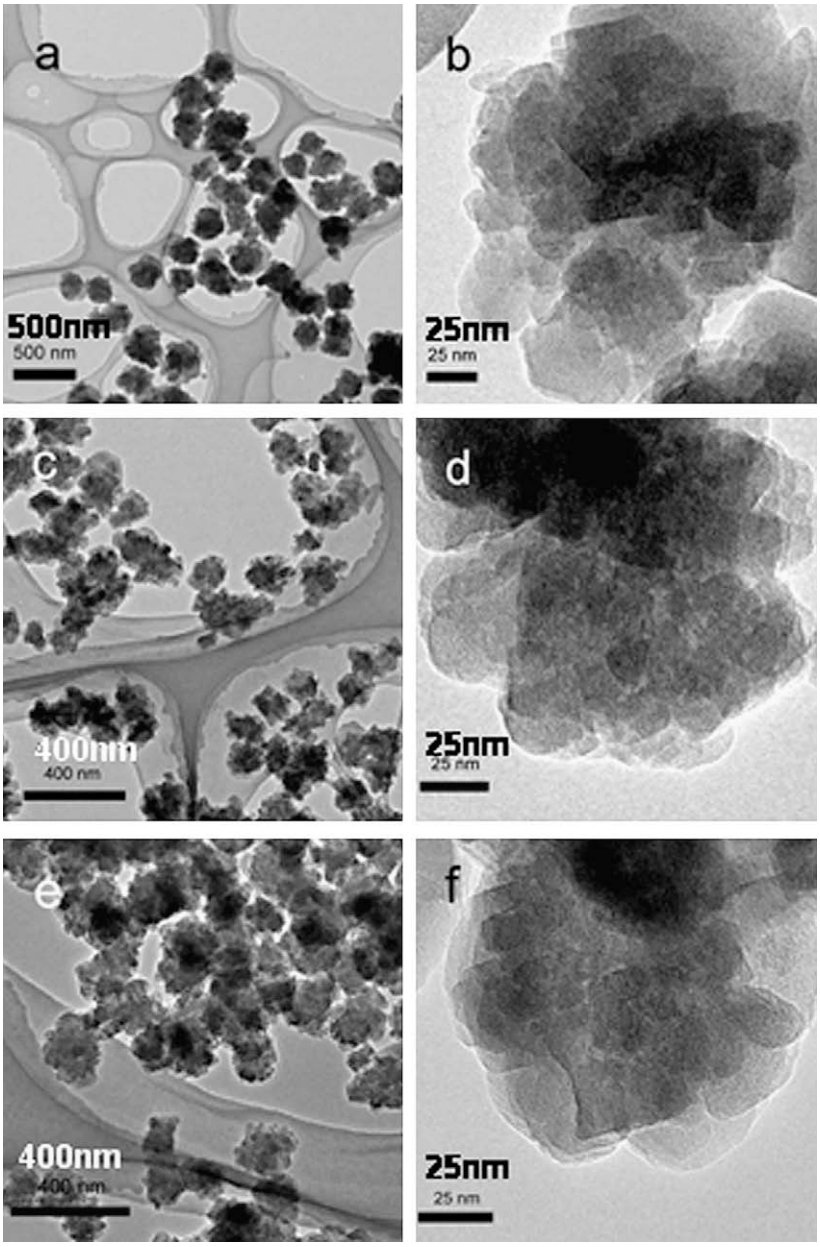

Fig. 8. TEM images of (a and b) Y-20.1H_2O, (c and d), Y-16.9H_2O and (e and f) Y-13.8H_2O.

tive, environmental friendly and scalable for the synthesis of hierarchical zeolite materials with tuneable size and controllable porosity.

Acknowledgments

This work was supported by the Australian National Research Flagships through Water for a Healthy Country Research Cluster and Australian Research Council. Y.H. thanks the CSIRO for the postgraduate scholarship. M.H. and A.H. acknowledge support from the CSIRO Science Leader Scheme.

References

[1] L. Tosheva, V.P. Valtchev, Chem. Mater. 17 (2005) 2494.
[2] A. Corma, Chem. Rev. 97 (1997) 2373.
[3] A. Corma, J. Catal. 216 (2003) 298.
[4] C.S. Cundy, P.A. Cox, Chem. Rev. 103 (2003) 663.
[5] V.P. Valtchev, K.N. Bozhilov, J. Phys. Chem. B 108 (2004) 15587.
[6] V.P. Valtchev, L. Tosheva, K.N. Bozhilov, Langmuir 21 (2005) 10724.
[7] H.T. Wang, B.A. Holmberg, Y.S. Yan, J. Am. Chem. Soc. 125 (2003) 9928.
[8] H.T. Wang, Z.B. Wang, Y.S. Yan, Chem. Commun. (2000) 2333.
[9] B.Z. Zhan, M.A. White, M. Lumsden, J. Mueller-Neuhaus, K.N. Robertson, T.S. Cameron, M. Gharghouri, Chem. Mater. 14 (2002) 3636.
[10] J.W. Song, L.M. Ren, C.Y. Yin, Y.Y. Ji, Z.F. Wu, J.X. Li, F.S. Xiao, J. Phys. Chem. C 112 (2008) 8609.
[11] M. Estermann, L.B. McCusker, C. Baerlocher, A. Merrouche, H. Kessler, Nature 352 (1991) 320.
[12] S. Mintova, N.H. Olson, V. Valtchev, T. Bein, Science 283 (1999) 958.
[13] N. Kuanchertchoo, S. Kulprathipanja, P. Aungkavattana, D. Atong, K. Hemra, T. Rirksomboon, S. Wongkasemjit, Appl. Organomet. Chem. 20 (2006) 775.
[14] G.S. Zhu, S.L. Qiu, J.H. Yu, Y. Sakamoto, F.S. Xiao, R.R. Xu, O. Terasaki, Chem. Mater. 10 (1998) 1483.
[15] J.F. Yao, H.T. Wang, K.R. Ratinac, S.P. Ringer, Chem. Mater. 18 (2006) 1394.
[16] J.F. Yao, L.X. Zhang, H.T. Wang, Mater. Lett. 62 (2008) 4028.
[17] R.W. Corkery, B.W. Ninham, Zeolites 18 (1997) 379.
[18] W. Song, V.H. Grassian, S.C. Larsen, Chem. Commun. (2005) 2951.
[19] V.P. Valtchev, A.C. Faust, J. Lezervant, Micropor. Mesopor. Mater. 68 (2004) 91.
[20] B.A. Holmberg, H.T. Wang, J.M. Norbeck, Y.S. Yan, Micropor. Mesopor. Mater. 59 (2003) 13.
[21] S. Mintova, N.H. Olson, T. Bein, Angew. Chem. Int. Ed. 38 (1999) 3201.
[22] W.G. Song, G.H. Li, V.H. Grassian, S.C. Larsen, Environ. Sci. Technol. 39 (2005) 1214.
[23] C. Pham-Huu, G. Wine, J.P. Tessonnier, M.J. Ledoux, S. Rigolet, C. Marichal, Carbon 42 (2004) 1941.
[24] I. Schmidt, A. Boisen, E. Gustavsson, K. Stahl, S. Pehrson, S. Dahl, A. Carlsson, C.J.H. Jacobsen, Chem. Mater. 13 (2001) 4416.
[25] I. Schmidt, C. Madsen, C.J.H. Jacobsen, Inorg. Chem. 39 (2000) 2279.
[26] Y. Huang, J. Ho, Z. Wang, P. Nakashima, A.J. Hill, H.T. Wang, Micropor. Mesopor. Mater. 117 (2009) 490.
[27] Y.S. Tao, H. Kanoh, K. Kaneko, J. Am. Chem. Soc. 125 (2003) 6044.
[28] M. Hartmann, Angew. Chem. Int. Ed. 43 (2004) 5880.
[29] A.H. Janssen, A.J. Koster, K.P. de Jong, Angew. Chem. Int. Ed. 40 (2001) 1102.
[30] P. Kortunov, S. Vasenkov, J. Karger, R. Valiullin, P. Gottschalk, M.F. Elia, M. Perez, M. Stocker, B. Drescher, G. McElhiney, C. Berger, R. Glaser, J. Weitkamp, J. Am. Chem. Soc. 127 (2005) 13055.
[31] S. van Donk, A.H. Janssen, J.H. Bitter, K.P. de Jong, Catal. Rev. Sci. Eng. 45 (2003) 297.
[32] J.C. Groen, W.D. Zhu, S. Brouwer, S.J. Huynink, F. Kapteijn, J.A. Moulijn, J. Perez-Ramirez, J. Am. Chem. Soc. 129 (2007) 355.
[33] H. Wang, T.J. Pinnavaia, Angew. Chem. Int. Ed. 45 (2006) 7603.
[34] M. Choi, H.S. Cho, R. Srivastava, C. Venkatesan, D.H. Choi, R. Ryoo, Nat. Mater. 5 (2006) 718.
[35] M. Kustova, K. Egeblad, K. Zhu, C.H. Christensen, Chem. Mater. 19 (2007) 2915.
[36] C.J.H. Jacobsen, C. Madsen, J. Houzvicka, I. Schmidt, A. Carlsson, J. Am. Chem. Soc. 122 (2000) 7116.
[37] W. Fan, M.A. Snyder, S. Kumar, P.S. Lee, W.C. Yoo, A.V. McCormick, R.L. Penn, A. Stein, M. Tsapatsis, Nat. Mater. 7 (2008) 984.
[38] W.C. Yoo, S. Kumar, Z.Y. Wang, N.S. Ergang, W. Fan, G.N. Karanikolos, A.V. McCormick, R.L. Penn, M. Tsapatsis, A. Stein, Angew. Chem. Int. Ed. 47 (2008) 9096.
[39] V. Naydenov, L. Tosheva, J. Sterte, J. Porous Mater. 12 (2005) 193.
[40] Y.C. Tong, T.B. Zhao, F.Y. Li, Y. Wang, Chem. Mater. 18 (2006) 4218.
[41] F.S. Xiao, L.F. Wang, C.Y. Yin, K.F. Lin, Y. Di, J.X. Li, R.R. Xu, D.S. Su, R. Schlogl, T. Yokoi, T. Tatsumi, Angew. Chem. Int. Ed. 45 (2006) 3090.
[42] H.T. Wang, L.M. Huang, Z.B. Wang, A. Mitra, Y.S. Yan, Chem. Commun. (2001) 1364.
[43] A.A. Dong, Y.J. Wang, Y. Tang, Y.H. Zhang, N. Ren, Z. Gao, Adv. Mater. 14 (2002) 1506.
[44] Y.J. Wang, Y. Tang, A.G. Dong, X.D. Wang, N. Ren, Z. Gao, J. Mater. Chem. 12 (2002) 1812.
[45] V. Valtchev, J. Mater. Chem. 12 (2002) 1914.
[46] Y.M. Fan, H.Q. Hu, G.H. Chen, Chem. Mater. 20 (2008) 1670.
[47] S.Y. Sang, Z.M. Liu, P. Tian, Z.Y. Liu, L.H. Qu, Y.Y. Zhang, Mater. Lett. 60 (2006) 1131.
[48] S.Y. Yang, A. Navrotsky, B.L. Phillips, Micropor. Mesopor. Mater. 46 (2001) 137.
[49] B. Fahlke, P. Starke, V. Seefeld, W. Wieker, K.P. Wendlandt, Zeolites 7 (1987) 209.
[50] H.J. Koroglu, A. Sarioglan, M. Tatlier, A. Erdem-Senatalar, O.T. Savasci, J. Cryst. Growth 241 (2002) 481.